Research Square

Preprints are preliminary reports that have not undergone peer review.
They should not be considered conclusive, used to inform clinical practice,
or referenced by the media as validated information.

# Sub-seasonal predictability of winter tornado regimes in Europe captured through disruptions to the stratospheric polar vortex

**Matthieu Lacroix**

matthieu.lacroix@univ-lyon2.fr

Université Lyon 2: Universite Lumiere Lyon 2 https://orcid.org/0009-0003-7049-486X

**Flavio Tiago Couto**

Universidade de Évora Centro de Estudos de História e Filosofia da Ciência: Universidade de Evora

**Yanni Gunnell**

Université Lyon 2: Universite Lumiere Lyon 2

**Research Article**

**Keywords:** Severe convection, Sub-seasonal to seasonal forecasting, Northern Annular Mode, Sudden Stratospheric Warming (SSW), East Atlantic Pattern, ERA5 Reanalysis

**Posted Date:** October 16th, 2026

**DOI:** https://doi.org/10.21203/rs.3.rs-10271149/v1

**License:** This work is licensed under a Creative Commons Attribution 4.0 International License.
Read Full License

# Abstract

Tornadoes and severe convective storms in Europe pose a significant yet historically under-recognised risk. Synoptic forecasting successfully captures severe convective environments at short lead times, but sub-seasonal to seasonal (S2S) predictability still remains limited. This study investigates the S2S modulation of European tornadic environments by stratospheric polar vortex disruptions, specifically major Sudden Stratospheric Warming (SSW) events. Departing from tornado environment indices (TEIs) elaborated in North America where convective and kinematic terms are multiplied, we calibrate an additive TEI suited to low-CAPE (convective available potential energy) European conditions using a Poisson Generalised Linear Model trained on European Severe Weather Database (ESWD) reports and ERA5 reanalysis. Applying this novel index to a 75-year climatology of cold-season tornadoes (1950–2025), we evaluate the lagged surface response to 50 major SSW events. We demonstrate that the downward-propagating Northern Annular Mode (NAM) signal does not yield a uniform response across the continent. Instead, the tropospheric impact is conditioned by the low-frequency East Atlantic (EA) pattern. During an EA-positive regime, SSW-induced equatorward jet displacement, coupled with warm, moist advection, doubles the baseline probability of extreme tornadic environments (up to + 15 percentage points) across southern Europe and around the Mediterranean Basin. In contrast, EA-negative regimes suppress instability across the entire continent as a result of atmospheric blocking. A combination of stratospheric monitoring with EA phase tracking thus provides a robust framework for anticipating high-impact European severe weather windows three to four weeks in advance.


# 1. Introduction

Tornadoes and severe convective storms affect Europe more frequently than commonly assumed. Despite a long-standing perception of the continent as being immune to the kinds of violent convection commonly reported from North America, the progressive harmonisation of the European Severe Weather Database (ESWD) has revealed a rich and geographically diverse tornado climatology, with several hundred confirmed tornado events reported annually across the continent (Groenemeijer and Kühne 2014; Antonescu et al. 2017; Lacroix et al. 2026a). Tornado occurrence clusters along preferred corridors linked to orography, coastlines, and the mean position of the North Atlantic jet stream, with distinct seasonal regimes emerging across different European sub-regions (Lacroix et al. 2026a).

The formation of tornadic environments requires the co-occurrence of (i) thermodynamic instability, typically measured by proxies such as convective available potential energy (CAPE), and (ii) sufficient kinematic forcing, usually expressed through vertical wind shear (Brooks et al. 2003; Taszarek et al. 2020). In Europe, however, these two components rarely reach the magnitudes observed in the North American Midwest, and their seasonal phasing differs markedly: warm-season events are thermodynamically driven, whereas cold-season tornadoes – which make up a large proportion of reported ≥F2-intensity events on the Fujita scale – occur in environments of low CAPE but anomalously strong low-level shear (Lacroix et al. 2026a). Predicting where and when either of these environmental

conditions will be met remains a significant forecasting challenge, particularly beyond the deterministic one-week forecast horizon.

Substantial progress has been made in understanding how large-scale tropospheric teleconnection patterns govern European severe weather regimes. The North Atlantic Oscillation (NAO), which is the leading mode of low-frequency atmospheric variability in the region, strongly dictates the interannual and multidecadal variability of severe convective environments (SCEs) by steering the North Atlantic jet stream and modulating the advection of warm, moist boundary-layer air into the continent (Lacroix et al. 2026b). However, purely tropospheric indices such as the NAO are limited in their predictive utility. The atmosphere is a chaotic system wherein tropospheric circulation anomalies typically decorrelate over a matter of days. Although the statistical relationships between NAO states and European tornadic environments are robust at synoptic timescales, extending the predictability of such environments beyond the typical 7-to-10-day limit remains a critical gap in operational meteorology. Forecasting ability at sub-seasonal to seasonal (S2S) timescales defines a poorly documented critical window for early warning systems and risk mitigation, but this requires looking beyond the troposphere and investigating the influence of more slowly evolving boundary forcing factors.

The stratosphere has emerged as a primary reservoir of S2S predictability for Northern Hemisphere weather regimes. The Northern Annular Mode (NAM) is the leading mode of extratropical atmospheric variability in the Northern Hemisphere, characterised by a zonally symmetric, or 'annular', pattern of geopotential height anomalies of opposite signs between the polar region and the mid-latitudes. The NAM encompasses the full depth of the atmosphere: its tropospheric expression is commonly referred to as the Arctic Oscillation (AO), and its stratospheric expression is a response to the variability of the stratospheric polar vortex. This vertical coherence makes the NAM a robust dynamic framework for understanding stratosphere–troposphere coupling (Thompson and Wallace 2000). During the boreal winter and early spring, the stratospheric polar vortex can experience profound, non-linear disruptions known as Sudden Stratospheric Warming events (SSWs). These are characterised by a rapid deceleration or complete reversal of the stratospheric Polar Night Jet and an abrupt spike in polar stratospheric temperatures, which can increase by 30–50°C or more over just a few days at altitudes between 10 and 50 km (Charlton and Polvani 2007). Crucially, the dynamical anomalies generated by SSWs do not remain confined to the middle or upper stratosphere. In the weeks following a major vortex disruption, strongly negative NAM anomalies often descend from the mid-stratosphere (e.g., 10 hPa level) to tropospheric levels – a phenomenon described as downward propagation (Baldwin and Dunkerton 2001).

When these downward-propagating anomalies couple with the troposphere, they enforce a persistent negative phase of the lower region of the NAM (i.e., the AO), effectively pushing the eddy-driven North Atlantic jet stream equatorward to anomalous positions for a duration of up to 60 days (Kidston et al. 2015). While the influence of this stratospheric driver of surface temperature anomalies, cold spells, and precipitation extremes in Europe is well documented in the climatological literature (Domeisen et al. 2020), its cascading impact on the highly specific, mesoscale atmospheric configurations required for

tornadogenesis remains undocumented. Furthermore, the atmospheric response to stratospheric forcing over Europe is rarely uniform, and is hypothesised to be highly sensitive to pre-existing tropospheric flow configurations.

Specifically, the East Atlantic (EA) pattern – often defined as the second leading mode of North Atlantic low-frequency variability after the NAO – acts as an important spatial modulator of European climate. Unlike the NAO, which is sensitive to action centres positioned over Iceland and the Azores, the EA is characterised by a single, zonally elongated centre of anomalous geopotential heights located over the central North Atlantic (approximately 50°N, 20–30°W), with no equivalent opposite-sign centre to its north. This configuration is effective at shifting North Atlantic storm tracks meridionally and significantly influences the subtropical branch of the jet stream and the influx of conditionally unstable air masses from the Mediterranean and subtropical Atlantic (Comas-Bru and McDermott 2014).

The hypothesis driving this study is that the geographical footprint of tornadic environments following a stratospheric vortex disruption event is governed by the phase of the EA pattern at the time of arrival of the stratospheric signal in the troposphere, leading to a highly state-dependent, synergistic response. Thus a negative surface NAM synchronous with a positive EA phase may yield a drastically different spatial distribution of CAPE and deep-layer shear (DLS) across western and central Europe compared to its occurrence during a negative EA phase (Piper et al. 2019).

Addressing this dynamic cascade quantitatively requires an objective metric. In the United States, researchers have successfully developed tornado environment indices (TEIs) using Poisson regression models to estimate the expected frequency of tornadoes based on specific combinations of CAPE and DLS or storm-relative helicity (SRH) (Tippett et al. 2012, 2014). These indices are inherently multiplicative: the convective and kinematic terms are combined as a product, such that the index approaches zero whenever either ingredient is absent. This formulation is physically justified in the North American context, where both thermodynamic instability and strong wind shear must co-occur for tornadic convection to be initiated. However, directly applying a North American TEI fails in the European context because of the aforementioned seasonal dichotomy detected by Lacroix et al. (2026a): during the cold season, near-zero CAPE would suppress the index to negligible values regardless of the intensity of ambient wind shear, rendering the index blind to the high-shear, low-CAPE (HSLC) environments that are responsible for a disproportionate share of significant European tornadoes. A bespoke metric is thus required, one that adopts an additive rather than multiplicative structure, allowing extreme winter shear to compensate for the absence or scarcity of thermodynamic instability and ensuring that HSLC tornado environments are captured across the full seasonal range of European severe convective activity.

By formulating an objectively calibrated European Tornado Environment Index (ETEI), it becomes possible to seamlessly track the temporal evolution of severe convective potential from the onset of a stratospheric disruption down to the surface. Furthermore, because the geographical footprint of European weather is highly sensitive to pre-existing patterns of tropospheric flow, evaluating how the

East Atlantic (EA) predictor modulates the spatial distribution of the ETEI during a stratospherically forced regime is ultimately fundamental.

The primary objective of this study is thus to develop a metric for European tornadic environments optimised for the 3-to-4-week forecasting window, and to investigate its sub-seasonal predictability following stratospheric polar vortex disruptions. Using ERA5 reanalysis data and historical ESWD reports, this research thus aims to:

1. calibrate and validate an additive European Tornado Environment Index (ETEI) – in which thermodynamic and kinematic terms contribute independently to the index rather than potentially cancelling each other out through multiplication. Under this new approach, extreme wind shear alone is sufficient to generate a high index value in the absence of high CAPE and should thus be capable of capturing the winter high-shear as well as the summer high-CAPE regimes previously highlighted by Lacroix et al. (2026a, b);
2. quantify the lagged response of this index to downward-propagating NAM anomalies following major SSW events;
3. evaluate how the phase of the East Atlantic (EA) pattern modulates the spatial distribution of hazardous tornadic environments at 3–4-week lead times.

## 2. Study area, data and methodology

# 2.1. Study area

The spatial domain for this study encompasses the European continent, the Mediterranean basin, and the eastern margins of the North Atlantic, explicitly defined by the bounding box 30°N–70°N and 25°W–45°E. This domain was deliberately selected to capture not only the primary regions of continental tornadogenesis documented in the ESWD, but also the critical upwind marine areas – notably the subtropical Atlantic and the Mediterranean Sea – that act as primary reservoirs of boundary-layer moisture and conditional instability for severe convection in Europe.

# 2.2. Sudden Stratospheric Warming detection

Major Sudden Stratospheric Warming (SSW) events were identified over the study period 1950–2025 using a three-source strategy, designed to account for the varying reliability of ERA5 reanalysis data across different observational eras (Hersbach et al. 2020).

For the radiosonde and satellite era (1958–2023) forming the core of the study, central dates were extracted directly from the NOAA Sudden Stratospheric Warming Compendium (SSWC; Butler et al. 2017), utilising the ERA5 dataset column. The SSWC applies the criterion defined by Charlton and Polvani (2007, hereafter CP07), whereby major SSW is defined as a reversal from westerly to easterly of the daily zonal-mean zonal wind at 10 hPa and 60°N during the extended boreal winter (November–March), with at least 20 consecutive days of westerly winds separating any two distinct events (Tripathi

et al. 2015). Five events listed in the SSWC were not detected in the ERA5 field (denoted by asterisks in the compendium) and were therefore excluded.

The resulting ERA5-based catalogue for 1958–2023 comprises 42 major SSW events, consistent with the expected frequency of 6.4 events per decade reported by Butler et al. (2017). While European tornadogenesis is demonstrably sustained during autumn and early winter through dynamically forced high-shear, low-CAPE (HSLC) environments (Lacroix et al. 2026a), the baseline ETEI climatology and subsequent composite analyses in this study are limited to the January–March (JFM) window. This time restriction is dictated by the climatological distribution of the stratospheric forcing itself, given that major SSW events predominantly cluster in mid to late winter. Restricting the baseline to JFM thus aligns the sub-seasonal lag window with the period of peak active coupling between the stratosphere and troposphere, thereby ensuring a robust statistical null-distribution used in bootstrap significance testing. The null distribution is constructed by repeatedly drawing random samples of JFM days from the climatological pool and computing their mean ETEI anomaly. The distribution thus obtained reflects the natural variability of the index under undisturbed winter conditions, thereby providing a physically consistent reference against which the true post-SSW composite anomaly is tested.

For the pre-catalogue period (1950–1957), the CP07 criterion was applied manually to ERA5 daily zonal-mean zonal winds at 10 hPa and 60°N. Because ERA5 stratospheric winds prior to the widespread availability of radiosonde observations are less reliably constrained (Bell et al. 2021), events detected during this period are explicitly flagged in the output catalogue and should be interpreted with appropriate caution. To exclude marginal reversals that would not meet the CP07 definition, an additional filter requiring at least five consecutive days of easterly winds was applied to rigorously exclude transient synoptic noise.

The reversal block was bounded to the extended winter season, i.e., the algorithm terminates each easterly block at the first day outside the November–March window, preventing the summer climatological easterly regime at 10 hPa from being erroneously incorporated. Consistent with the protocol established above, this extended detection window feeds into the restricted January–March analysis. Six events were identified for 1950–1957 using this procedure. Pending the release of an updated SSWC, the same algorithmic approach was applied to the post-catalogue period (2024–2025) and yielded two further events. The final consolidated catalogue comprises overall 50 major SSW central dates spanning 1950–2025 (Table S1).

# 2.3. Northern Annular Mode index

The Northern Annular Mode (NAM) index was computed following Baldwin and Thompson (2009) as the leading principal component (PC1) of daily geopotential anomalies poleward of 20°N. This was calculated independently for each of ten pressure levels: 10, 30, 50, 100, 200, 300, 500, 700, 850, and 1000 hPa.

Daily geopotential anomalies were obtained by subtracting a long-term calendar-day mean from the raw ERA5 geopotential field. For each grid point and pressure level, this reference mean was computed as the calendar-day mean over the full study period, then smoothed using a 30-day Hann window applied circularly across the day-of-year axis to eliminate discontinuities at year boundaries while preserving the seasonal cycle.

Empirical Orthogonal Function (EOF) analysis was used to decompose the consolidated dataset into orthogonal spatial patterns and associated time series, thereafter allowing for the identification of dominant variability patterns. To avoid contaminating the EOF spatial patterns with the less reliably constrained pre-satellite ERA5 stratospheric data (Hersbach et al. 2020; Bell et al. 2021), EOF analysis was performed exclusively on the satellite era data (1979–2025). At each pressure level, the leading EOF was derived via an incremental covariance matrix formulation to ensure computational efficiency. Prior to covariance accumulation, anomalies were weighted by the square root of the cosine of latitude to account for the convergence of meridians (North et al. 1982). The symmetric covariance matrix was then decomposed using a truncated symmetric eigendecomposition routine and retaining only the leading eigenpair.

For the pre-satellite period (1950–1978), daily geopotential anomalies were projected onto the satellite-era EOF1 spatial pattern rather than recomputing the EOFs from the earlier data. This approach, recommended by Baldwin and Thompson (2009), ensures temporal consistency of the NAM index across the full study period while anchoring the spatial structure of the mode to the observationally better-constrained satellite era. The sign convention was enforced such that a negative NAM index corresponded to a positive geopotential anomaly over the polar cap (poleward of 65°N), indicative of a weakened stratospheric polar vortex. The final PC1 time series at each level was standardised to zero mean and unit standard deviation.

## 2.4. Hovmöller composite diagram

To characterise the downward propagation of the stratospheric NAM signal following major SSW events (the primary physical mechanism underpinning the S2S predictability signal exploited in this study), a lagged composite of the three-dimensional NAM index was constructed, centred on each of the 50 SSW central dates. The composite window spans 30 days prior (T–30) to 60 days following (T + 60) the central date (T = 0). At each lag interval and pressure level, the composite value represents the unweighted ensemble mean (i.e., arithmetic average) of the NAM index across all 50 events.

Statistical significance was assessed using a non-parametric block bootstrap procedure with 500 resamples. For each resample, an equivalent number of dates ($n$ = 50) was drawn at random from the full time series, subject to the constraint that the lag window did not extend beyond the temporal bounds of the dataset. The composite mean was recomputed for each random draw, generating an empirical null distribution of NAM anomalies under the assumption of no coherent stratospheric forcing. A grid cell (lag × pressure level) was deemed statistically significant at the 5% level ($\alpha$ = 0.05) if the observed composite fell outside the 2.5th–97.5th percentile bounds of the bootstrap distribution.

## 2.5. European Tornado Environment Index (ETEI) calibration and reconstruction

To evaluate the sub-seasonal to seasonal (S2S) predictability of European tornadic environments driven by stratospheric forcing, a continuous daily proxy representing severe convective potential is required. Given the inherent spatial and temporal reporting biases in historical tornado databases until the end of the 20th century (see discussions about data detrending in Lacroix et al., 2026a, b), a gridded index encoding the statistical likelihood of tornado occurrence as a function of local atmospheric conditions – named here the European Tornado Environment Index (ETEI) – was calibrated over a reliable modern observation period and subsequently applied to reanalysis data to generate a 75-year climatological reconstruction (1950–2025).

### 2.5.1. Predictor variable processing

Atmospheric parameters representing thermodynamic instability and kinematic organisation were extracted from the ERA5 reanalysis dataset. Surface-based convective available potential energy (CAPE) was utilised as the primary thermodynamic predictor. To quantify the kinematic environment, two distinct wind shear proxies were calculated:

1. Deep-layer shear (DLS): a proxy for the 0–6 km bulk shear, computed here as the vector difference between the 500 hPa and 1000 hPa horizontal wind fields.
2. Low-level shear (LLS): a proxy for the 0–1 km bulk shear, calculated as the vector difference between the 925 hPa and 10 m horizontal wind fields.

Because extreme convective environments frequently exhibit strong diurnal cycles, the daily maximum values of CAPE, DLS, and LLS were computed across the four primary synoptic hours (0000, 0600, 1200, and 1800 UTC). To ensure robust statistical modelling and align with the spatial scale of synoptic features, the ERA5 variables (originally at 0.25° resolution) were regridded to a 2° × 2° grid. This spatial coarsening acts as a low-pass filter, damping mesoscale noise to better isolate the synoptic-scale environmental background state modulated by planetary-scale teleconnections. Importantly, rather than averaging the variables – which would artificially dilute highly localised extreme environments – the spatial maximum of each predictor within the 2° grid cell was retained. All predictors were standardised (using *z*-scores) prior to regression to ensure numerical stability.

### 2.5.2. Poisson GLM calibration and model selection

Tornado occurrence data were retrieved from the European Severe Weather Database (ESWD). To minimise the impact of tornado under-reporting, the calibration period was strictly limited to 2005–2020, retaining only reports that successfully passed the ESWD quality control protocols (QC0+) and had been assigned a Fujita intensity rating of F0 or higher. The filtered reports were aggregated onto the 2° × 2° spatial grid, generating a daily two-dimensional histogram of tornado cell-days.

Following established methodologies for defining tornado environment proxies (Tippett et al. 2012, 2014), which are addressed as discrete, non-negative integer events conforming to a Poisson probability distribution, a Poisson Generalised Linear Model (GLM) was employed to associate the expected daily tornado count (λ) in each 2° × 2° grid cell with the ERA5 environmental predictors via a log-linear link function.

To determine the most physically representative formulation for the European domain, a sensitivity analysis was conducted by training three competing GLM configurations, each combining a thermodynamic term and a kinematic term in a different structural arrangement. In all three formulations, subscript *z* denotes that the predictor variables have been standardised to zero mean and unit variance over the calibration period (and thus expressed as *z*-scores) so as to render the regression coefficients directly comparable across predictors of differing physical units and magnitudes, and to distinguish this standardisation notation from the vertical coordinate *z* used elsewhere in the paper. Model A incorporated deep-layer shear (DLS) with a multiplicative interaction term between the thermodynamic and kinematic predictors. Models B and C both relied on low-level shear (LLS, 0–1 km), with Model B retaining the multiplicative interaction term and Model C adopting a purely additive structure in which the two predictors contribute independently to the index. Model selection was governed by the Akaike Information Criterion (AIC), and the comparative performance of the three configurations is reported in Section 3.1.

The three competing formulations differ solely by the choice of kinematic predictor and in the structural relationship – multiplicative or additive – between the thermodynamic and kinematic terms:

- Model A (Deep Shear, Interactive): $loglog\ (\lambda\ )\ \sim\ CAPE_z + DLS_z + (CAPE_z \times\ DLS_z)$
- Model B (Low-Level Shear, Interactive): $loglog\ (\lambda\ )\ \sim\ CAPE_z + LLS_z + (CAPE_z \times\ LLS_z)$
- Model C (Low-Level Shear, Additive): $loglog\ (\lambda\ )\ \sim\ CAPE_z + LLS_z$

# 2.5.3. Historical ETEI reconstruction

Based on the superior performance of Model C, the final ETEI formulation was defined as the log-transformed expected rate derived from the purely additive Poisson GLM:

$$ETEI \propto\ -1.87 + 0.40 \cdot\ CAPE_z + 0.44 \cdot\ LLS_z$$

Both main effect coefficients were highly significant ( $p < 10^{-90}$). This equation was applied vectorially to the full ERA5 dataset to reconstruct a continuous, daily 2° × 2° gridded climatological reconstruction of the ETEI from 1950 to 2025. Finally, the daily ETEI grids were standardised (mean of 0, standard deviation of 1) across the full temporal domain to facilitate the analysis of lagged composites following Sudden Stratospheric Warming (SSW) events.

## 2.6. Stratosphere–troposphere coupling and lagged ETEI composites

To quantify the sub-seasonal impact of stratospheric vortex disruptions on severe weather risk at ground level, a lagged composite analysis of the reconstructed ETEI was performed. Guided by the temporal scale of the downward-propagating Northern Annular Mode signal observed in the Hovmöller analysis, a specific sub-seasonal to seasonal (S2S) lag window of 15 to 30 days following the SSW central date (T + 15 to T + 30) was selected for evaluation. Based on preliminary distribution testing, the 80th percentile of the ETEI was established *a priori* as the critical threshold for defining highly conducive tornadic environments in our subsequent sub-seasonal composite analyses.

### 2.6.1. Mean composites and climatology

For the domain-averaged temporal analyses and the regime-stratified composites, an aggregate SSW composite was constructed by averaging the ETEI spatial fields across the target lag windows. To isolate the stratospheric forcing signal, an ETEI anomaly field was computed by subtracting the long-term climatological mean. The baseline atmospheric pattern was defined using only the late-winter to early-spring window (January–March) from 1950 to 2025, deliberately excluding any 60-day window that might follow a SSW central date to prevent signal contamination within the null background state.

### 2.6.2. Peak exceedance probability (P90)

Given that standard mean composites can mathematically smooth over highly non-linear convective extremes, for example by cancelling out days of severe tornadic potential with days of strong anti-cyclonic suppression, the broader spatial footprint of the SSW response was evaluated using a peak exceedance probability approach. At first, the local 90th percentile (P90) of the ETEI was calculated independently for each 2° × 2° grid cell using the long-term reference distribution of winter ETEI values, constructed from JFM days falling outside the asymmetric exclusion windows (–30 to + 60 days relative to the SSW central date). The probability of exceeding this local P90 threshold during the specific lag windows was subsequently computed across all 50 SSW events. The resulting spatial anomaly was expressed in percentage points relative to the baseline climatological probability of 10%.

### 2.6.3. Bootstrap significance testing

The statistical significance of both the mean spatial anomalies and the P90 exceedance probabilities was evaluated using a 1000-iteration Monte Carlo bootstrap procedure applied independently to each grid cell.

For the mean anomaly composites, a random sample of *N* continuous, 16-day blocks was drawn from the long-term JFM reference period to build the empirical null distribution. For the P90 exceedance maps, the null distribution was constructed by randomly drawing an equivalent number of individual days from the JFM daily ETEI time series, excluding the asymmetric exclusion windows surrounding each

SSW central date, and calculating their random exceedance fraction. The observed SSW anomalies were deemed statistically significant at the 95% confidence level ($\alpha$ = 0.05, two-tailed) if they fell outside the 2.5th–97.5th percentile bounds of their respective local null distributions.

## 2.7. Tropospheric teleconnection modulation by the East Atlantic pattern

The downward-propagating stratospheric signal does not act on a passive troposphere: its surface expression is, instead, heavily modulated by the pre-existing background synoptic flow. Whereas the North Atlantic Oscillation (NAO) primarily governs the latitudinal position of the eddy-driven jet, the East Atlantic (EA) pattern strongly controls the meridional advection of warm, moist air masses from the Mediterranean and Iberian Peninsula northward into continental Europe – a primary requisite for the development of severe convective instability.

To assess this non-linear modulation, the 50 SSW events were stratified according to the background state of the EA pattern. The historical monthly EA index was obtained from the NOAA Climate Prediction Center and mapped to a daily frequency scaling with the ETEI dataset. For each SSW event, the mean EA index was calculated specifically within the target S2S window (T + 15 to T + 30).

The SSW catalogue was subsequently partitioned into two distinct regimes: events coinciding with a positive EA phase (mean index > 0) and events coinciding with a negative EA phase (mean index ≤ 0). Lagged ETEI anomaly composites were recomputed independently for both the EA-positive and EA-negative sub-samples. To ensure rigorous statistical validation despite the limited sample sizes, the pixel-by-pixel Monte Carlo bootstrap test (Section 2.5) was applied independently to each sub-sample, with the resampling parameter *N* dynamically adjusted to match the exact number of events under the respective EA regimes.

# 3. Results

## 3.1. Calibration and climatology of the ETEI

The Poisson GLM sensitivity analysis reveals a clear dependency of European tornadic environments on low-level kinematics rather than on deep-layer processes (Fig. 1A, Calibration and spatial validation of the European Tornado Environment Index (ETEI). (A) Model selection using the Akaike Information Criterion (AIC) across three Generalized Linear Model (GLM) configurations. The purely additive Model C yields the lowest AIC, demonstrating superior performance over multiplicative and formulations involving deep-layer shear. Key to acronyms – CAPE: convective available potential energy; DLS: dee-layer shear, LLL: low-level shear. (B) Long-term climatological mean of the standardised ETEI across the European and Mediterranean domain. Positive values (warm colours) delineate broad regions with an elevated baseline risk for tornadogenesis, whereas negative values (cool colours) highlight unfavourable environments. Black dots locate F ≥ 0-intensity ESWD tornado reports of recorded during January–March over the 2000–2023 period (n = 1010). (C) Conditional probability of significant tornadoes (F ≥ 2) per

1,000 grid cell-days as a function of ETEI percentiles, computed over the independent 2021–2022 test period. The distribution reveals a sharp, non-linear escalation in tornado probability for environments exceeding the 80th percentile (red bars).). Model A, which incorporates 0–6 km deep layer shear (DLS), is substantially outperformed by Model B, which utilises 0–1 km low-level shear (LLS), as evidenced by a reduction in the Akaike Information Criterion from 10538 to 10344 (ΔAIC = 194), far exceeding the threshold of ΔAIC > 10 conventionally interpreted as very strong evidence against the higher-AIC model (Burnham and Anderson 2002). This result corroborates recent European climatological studies emphasising the primacy of 0–1 km rotational and kinematic fields for tornadogenesis (e.g. Púčik et al. 2015; Taszarek et al. 2020; Lacroix et al. 2026a). Furthermore, the multiplicative interaction term between instability and shear within Model B yields a statistically non-significant coefficient (p = 0.868), indicating that the two predictors do not act synergistically in the European context. Removing this interaction term yields the purely additive Model C, which achieves the lowest overall AIC (10342) and thus provides the optimal balance of goodness-of-fit and parsimony. This additive structure is physically consistent with the European climatological regime, i.e., where environments simultaneously exhibiting extreme thermodynamic instability and extreme low-level shear are considerably rare by comparison with the North American Midwest.

In the final selected model (Model C), the standardised main effects of $CAPE_z$ (coefficient = 0.40) and $LLS_z$ (coefficient = 0.44, see tests in section 2.5.2) were of comparable magnitude and both highly significant (p < 0.001). This confirms that thermodynamic instability and low-level rotation act as independent, equally critical requisites for tornadogenesis in Europe, and distinguishes the European atmospheric setting from the highly interactive severe weather environments more typical of North America.

The spatial fidelity of the reconstructed ETEI is validated by its long-term climatological mean (Fig. 1B). The index accurately captures the established geographical distribution of severe convective risk across the continent. Black dots locate F ≥ 0-intensity ESWD tornado reports of recorded during January–March over the 2000–2023 period (n = 1010). Rather than highly localised hotspots, the reconstructed climatology delineates a clear regional dichotomy: (i) broad, continuous zones of elevated baseline risk (mean ETEI values ranging from + 0.58 to + 0.87) are well defined over the Po Valley in northern Italy, the western and southern coastal lowlands of France, the Benelux region and northern Germany, the British Isles and Ireland, and the coastal Mediterranean Basin. These favourable corridors strongly contrast with (ii) unfavourable environments (ETEI < − 0.58) positioned over major orographic barriers (e.g., Alps, Scandes, Atlas Mountains), higher latitudes, elevated plateaus such as the central Iberian Meseta, central Turkey and marine and continental areas dominated by anticyclonic regimes (e.g., the subtropical Atlantic). The cluster of reports along the Portuguese and southwestern Spanish coastlines, situated at the transitional boundary between positive and near-zero ETEI values, is consistent with the prevalence of dynamically forced, high-shear low-CAPE tornado environments along this coastline during the cold season, as documented by Lacroix et al. (2026b). Crucially, the reliability of the ETEI as a forecasting proxy for high-impact severe weather is demonstrated over the independent test period of 2021–2022 showcased here (Fig. 1C). With the exception of a minor statistical artefact at the 20th percentile – likely

representing a rare outlier event driven by highly localised, sub-grid mesoscale boundaries unresolved at the 2° synoptic resolution – the conditional probability of a significant tornado (F ≥ 2) remains virtually negligible for environments extending below the 60th percentile. However, the probability exhibits a sharp, non-linear escalation within the upper percentiles, peaking above the 80th and 90th percentiles. This exponential threshold response confirms that high positive ETEI anomalies effectively isolate the rare atmospheric background states conducive to intense tornadogenesis, making the index a robust tool for sub-seasonal composite analysis.

# 3.2. Downward propagation of the stratospheric signal

Based on the consolidated catalogue of 50 major SSW events detailed in section 2.1, the temporal distribution of these disruptions (Fig. 2A, Chronology and downward propagation of major Sudden Stratospheric Warming (SSW) events. (A) Annual frequency of the 50 major SSW central dates identified during the extended winter season across the 1950–2025 period (see Table 1). Vertical dashed lines delineate methodological transitions: the pre-catalogue era (orange bars), the core NOAA SSWC dataset spanning the pre-satellite and satellite eras (blue bars, 1958–2023), and the manually appended post-catalogue period (yellow bars, 2024–2025). (B) Pressure–time cross-section illustrating the lagged composite of the standardised Northern Annular Mode (NAM) index centred on the SSW occurrence (T = 0, vertical dashed line). The composite spans from 30 days prior to 60 days following the central date. Deep blue shading indicates robust negative NAM anomalies propagating downward from the middle stratosphere (10 hPa) to the lower troposphere (1000 hPa). Solid black contours enclose regions of statistical significance at the 95% confidence level ($p < 0.05$), determined via a 500-resample non-parametric block bootstrap procedure.) highlights pronounced interannual variability, with some decades exhibiting frequent warming events whereras others experience prolonged absences of SSW.

To evaluate the dynamic coupling between these stratospheric disruptions and the troposphere, the lagged composite of the Northern Annular Mode (NAM) index was analysed (Fig. 2B). The Hovmöller diagram displays here the characteristic signature of a major SSW in the upper levels: a profound and highly significant negative NAM anomaly $(\leq -1.5\,\sigma)$ emerges in the mid-to-upper stratosphere (10–50 hPa) coincident with the central date (T = 0). This regime, indicative of a collapsed and anomalously warm polar vortex, exhibits immense inertia and persists robustly for over 40 days.

The composite illustrates the classic ‘dripping paint’ effect, whereby this negative NAM anomaly propagates downward through the lower stratosphere, crossing the nominal tropopause (indicated at 100 hPa) within the first 10 days following the central date. However, the signal attenuates as it reaches the lower troposphere (850–1000 hPa). While a weak shift towards a negative NAM state is visible near the surface immediately after T = 0, the solid black contours indicating 90% statistical significance do not extend into the boundary layer in a sustained manner. After T + 10, the surface signal becomes patchy and statistically indistinguishable from background climatological noise.

The absence of a robust, uniform surface response across the unstratified 50-event SSW array is a key finding. It suggests that while the stratospheric signal systematically reaches the upper troposphere, its

translation into a surface weather regime is not guaranteed. The downward-propagating anomaly is likely to be either arrested by strong internal tropospheric dynamics or heavily modulated by competing synoptic background states, such as the pre-existing configuration of North Atlantic and European storm tracks.

### 3.3. Sub-seasonal response of tornadic environments

To quantify the direct tropospheric impact of stratospheric forcing, the reconstructed ETEI was initially aggregated across all 50 major SSW events in an unstratified bulk analysis. The temporal evolution of the domain-averaged anomaly (Fig. 3, Evolution over time of the domain-averaged ETEI anomaly following major Sudden Stratospheric Warming (SSW) events. Solid red curve illustrates the lagged composite of the European Tornado Environment Index (ETEI) anomaly, expressed in standard deviations (σ), spanning from 15 days prior to 60 days following the SSW central date (T = 0, vertical black line). The composite is derived from 50 major events restricted to the January–March (JFM) window between 1950 and 2025. Horizontal light blue band represents the 95% confidence interval of the climatological null background state, computed via a two-tailed bootstrap resampling procedure. Red circular markers along the curve denote daily values that are statistically significant at the 95% confidence level ($p < 0.05$). The vertical red shaded region highlights the target sub-seasonal predictability window (weeks 3 and 4; T + 15 to T + 30), corresponding to a sustained and statistically robust suppression of tornadic environments across the European domain.) reveals a general suppression of tornadic potential across the broader European domain, turning negative immediately after the central date and reaching its minimum during the third and fourth weeks (T + 15 to T + 30 days). However, evaluating the spatial structure of this response using a standard composite mean (Suppl. Fig. S1) yields largely non-significant results over the continent. This lack of significance occurs because the standard mean attenuates the physical signal by averaging opposing tropospheric responses and smoothing spatial extremes.

Across northern continental Europe, Scandinavia, and the British Isles, the probability of encountering a P90 tornadic environment drops by up to 10 percentage points (e.g., Fig. 4C, D). Given the 10% climatological baseline, this indicates a near-complete suppression of severe convective potential in these regions. This observation is consistent with the equatorward shift of the eddy-driven jet and the establishment of cold, stable continental blocking regimes.

Conversely, a robust and statistically significant enhancement emerges over the Mediterranean Basin, southern Italy, the Balkans, and North Africa. In these southern regions, the probability anomaly gains 10 to 12 percentage points. This effectively doubles or even triples the baseline risk of extreme tornadic environments (shifting from the 10% baseline to 20–25% exceedance probability), driven by the intensified kinematic shear supplied by the displaced polar jet.

While the P90 exceedance maps successfully uncover this latitudinal dipole, the signal remains mixed and largely non-significant over transitional zones, including western and central Europe. The event-by-event distribution of the domain-mean ETEI anomalies (Fig. 5, Distribution of domain-mean ETEI

anomalies per SSW event, stratified by lag week. Each violin plot represents the kernel density estimation of ETEI anomalies (in σ units) for the 50 major SSW events identified between 1950 and 2025. Dark grey circles denote individual event anomalies, while the horizontal red bars indicate the weekly median value. The region shaded in pale red highlights the target sub-seasonal window (weeks 3 and 4; T + 15 to T + 28), where median suppression of tornadic potential is most pronounced. The substantial vertical spread of data points within each 'violin' demonstrates the significant inter-event variance inherent to the stratosphere–troposphere coupling process, confirming that the sub-seasonal response to SSW events is not uniform and remains highly conditional on the tropospheric background state.) provides the necessary context, showing that the sub-seasonal response exhibits substantial inter-event variance. Although the median anomaly confirms an overall domain-wide suppression reaching its lowest point during Week 4, individual SSW events produce anomalies ranging from highly suppressed ( $\leq -0.5\,\sigma$ ) to exceptionally elevated ( $\geq +0.3\,\sigma$ ) during Week 5.

This considerable event-to-event spread demonstrates that while the downward-propagating stratospheric signal systematically alters the latitudinal position of the jet stream, its ultimate translation into extreme convective risk over continental Europe is not deterministic. Instead, it indicates that the surface expression of any given SSW is strongly modulated by the pre-existing, low-frequency background state of the troposphere, making the interaction with regional teleconnections – such as the East Atlantic (EA) pattern – a necessary subsequent step for analysis.

# 3.4. Tropospheric modulation by the East Atlantic pattern

To resolve the high inter-event variance and identify the dynamic pathways governing the surface response, the 50 major SSW events were stratified according to the contemporaneous background state of the East Atlantic (EA) pattern. Excluding the March 2025 event (pending index publication), the catalogue was partitioned into 26 EA-positive events and 23 EA-negative events.

The stratified time series of the domain-averaged ETEI anomalies (Fig. 6 Stratified temporal evolution of domain-mean ETEI anomalies following major SSW events. The time series illustrates the response of tornadic potential (in σ units) to 50 major SSWs, partitioned by the background state of the East Atlantic (EA) pattern. Black dashed line: bulk composite (all events). Red and blue lines: EA-positive (n = 26) and EA-negative (n = 23) regimes, respectively. The central date of the SSW is marked at T = 0. Shaded orange window (T + 15 to T + 30 days) highlights the sub-seasonal interval where the divergence between the two EA regimes is most pronounced, demonstrating that the EA-negative phase is the primary driver of the broader continental ETEI suppression observed in the bulk analysis.) clarifies the origin of the continental suppression noted in the bulk analysis. The pronounced decrease in the domain average during the Week 3 and Week 4 windows (T + 15 to T + 30) is predominantly driven by the EA-negative regime. In contrast, the EA-positive regime maintains a domain-mean state much closer to neutral, effectively masking competing regional anomalies.

The spatial composites for the target sub-seasonal window (Fig. 7) reveal a clear physical dichotomy, indicating that the EA phase modulates the downward-propagating stratospheric signal. Under EA-

positive conditions (Fig. 7, left panel), the interaction between the SSW-induced equatorward jet shift and the background EA flow generates a highly amplified pattern. As visually evident in the composite, a statistically significant positive ETEI anomaly emerges predominantly along the coastal margins, specifically over Portugal, Spain, and the Atlantic seaboard of France. This signal extends eastward into the Po Valley and across the broader Mediterranean Basin including northern Algeria, where anomaly values reach + 0.3 $\sigma$. The statistical robustness of this regional enhancement across the Western Mediterranean is explicitly confirmed by spatial bootstrap testing (Suppl. Fig. S2), demonstrating that this sub-seasonal concentration of tornadic environments is a persistent dynamic feature rather than a sampling artefact. This configuration facilitates the advection of warm, moist Mediterranean and subtropical Atlantic air masses, coupling thermodynamic instability with the enhanced kinematic shear provided by the displaced jet stream. For these regions, the occurrence of a Sudden Stratospheric Warming event during an EA-positive phase effectively preconditions the environment for severe convection. Crucially, this theoretical peak in environmental potential is corroborated by observational evidence: ESWD tornado reports over the southern European domain show a high frequency of occurrence during T + 15 to T + 30 following EA-positive SSW events (Suppl. Fig. S3), lending observational support to the sub-seasonal predictability signal identified by the ETEI composite. Simultaneously, this amplified flow induces a pronounced suppression of tornadic potential across northern and central Europe, with values attaining − 0.4 $\sigma$. This zone of negative ETEI anomalies also extends southward into specific regional corridors, notably the Rhône Valley, highlighting the steep spatial gradients arising from by this atmospheric regime.

Conversely, under EA-negative conditions (Fig. 7, right panel) the spatial response shifts entirely equatorward. The negative ETEI anomalies, limited to Scandinavia in the EA-positive composite, now cover most of the European continent, with values ranging between − 0.4 and 0 $\sigma$. This widespread suppression results from persistent continental blocking and the advection of cold, dry polar air, which inhibits the CAPE-dependent thermodynamic instability essential for triggering severe convection.

The composite, however, shows that the tornadic threat is not extinguished but merely displaced. A distinct corridor of positive ETEI anomalies develops along the coast of North Africa, from the Maghreb to Egypt, and reaches into the eastern Mediterranean and the Levant. Here, the SSW-induced jet displacement, combined with the EA-negative background state, forces the active baroclinic zone unusually far south, with anomaly values reaching + 0.2 $\sigma$ over the eastern Mediterranean. The resulting concentration of kinematic shear creates a localised window of elevated risk in these southern regions, while the rest of continental Europe remains under a stable, inhibited regime.

## 4. Discussion

# 4.1. Conditional nature of stratosphere–troposphere coupling

The zonal wind reversal criteria used to identify major Sudden Stratospheric Warming events (section 2.2) are conceived to isolate periods of peak active coupling between the stratosphere and troposphere. In classic sub-seasonal dynamics, the downward propagation of this stratospheric signal is expected to reliably force an equatorward shift of the tropospheric eddy-driven jet stream and increase blocking over high latitudes (Baldwin and Dunkerton 2001). However, the spatial responses presented in Section 3 challenge the deterministic assumption that this stratospheric forcing translates uniformly into a single, predictable severe weather regime across Europe.

The near absence of spatial anomalies observed in the unstratified bulk composite analysis initially obscured the actual surface impact of SSW events. Data stratification calibrated on variations in the East Atlantic (EA) pattern (Fig. 7), however, reveals instead that stratosphere–troposphere coupling is strictly conditional. A polar vortex disruption does not unilaterally generate tornadic environments but rather acts as a kinematic amplifier, the final expression of which is modulated by the thermodynamic background state of the lower troposphere. Consequently, the SSW modulates rather than generates the existing baroclinic zones, thereby highlighting the tropospheric, EA-conditioned background state as the primary constraint on tornadogenesis.

This conditional response can be explained through an ingredients-based framework for deep moist convection (Doswell et al. 1996; Schultz et al. 2000). Tornadogenesis requires the spatial superposition of robust, CAPE-driven thermodynamic instability and strong low-level vertical wind shear (LLS). Following a Sudden Stratospheric Warming event, the equatorward displacement of the polar jet stream systematically enhances the background wind shear over central and southern Europe. However, shear alone cannot trigger deep convection if the boundary layer lacks buoyancy and moisture: influence from the East Atlantic pattern is critical. The EA interferes in the following way:

1. During an EA-positive regime, the tropospheric circulation is dominated by an anomalous south-westerly flow that advects maritime moisture and warm air from the subtropical Atlantic and the Mediterranean basin into continental Europe. When the SSW-induced jet displacement overlaps with this thermodynamically primed boundary layer, it provides the required dynamic trigger. This coupling explains the statistically significant increase in values of the European Tornado Environment Index (ETEI), particularly over the Iberian Peninsula, southern France, and the Po Valley.
2. During an EA-negative regime, the dominant surface flow is characterised by continental blocking or anomalous northerlies. This circulation drives cold, dry polar or continental air masses across Europe, restricting the low-level moisture required to build CAPE. Under these conditions, although the SSW still shifts the polar jet equatorward – a characteristic feature of the stratospheric downward influence (Baldwin and Dunkerton 2001; Domeisen et al. 2019) – the enhanced kinematic shear acts upon a stable atmosphere. The severe convective risk is therefore suppressed across the continent.

These findings demonstrate that while stratospheric forcing primarily modulates the kinematic environment (shear) conducive to European severe weather, the low-frequency tropospheric background

state (the EA pattern) enables the thermodynamic environment (instability). Accounting for this synergistic, conditional interaction, which is also consistent with recent research highlighting the complex spatio-temporal nature of stratosphere–troposphere coupling (Yu et al. 2022), is essential for translating stratospheric anomalies into actionable sub-seasonal severe weather forecasts.

## 4.2. Regional contrasts: European vs. North American climatology

The dynamics governing European severe convective environments reveal distinct regional characteristics compared to the North American Midwest. In the United States, the modulation of tornadic risk is often strongly coupled with tropical teleconnections, notably the El Niño–Southern Oscillation (ENSO), and is driven by large-scale synoptic disturbances that articulate deep-layer shear (DLS) with extreme instability in a highly interactive, non-linear fashion (Tippett et al. 2012).

Our analysis for Europe highlights a fundamentally different regime. The superior performance of the additive Model C, where CAPE and LLS contribute independently, and the statistical insignificance of their interaction, suggest that the 'explosive' overlap of parameters is much more infrequent at European mid-latitudes than in the U.S. Furthermore, our findings emphasise the dominance of low-level kinematic organisation (low-level shear, in particular) over deep-layer processes. This concurs with the physical reality of European tornadogenesis, which frequently occurs in high-shear, low-CAPE environments (Brooks et al. 2003; Groenemeijer and Kühne 2014; Lacroix et al. 2026a, b). These systems often manifest as quasi-linear convective systems (QLCS) rather than as the long-lived, discrete supercells that define the American tornado paradigm. Given that the application of U.S.-centric proxies often fails to capture the specific kinematic sensitivities that define severe convective risk in the European and Mediterranean regions, these regional idiosyncrasies reinforce the necessity of tailoring sub-seasonal indices specifically for the European domain.

## 4.3. Methodological limitations and future considerations

While the ETEI provides a robust proxy for long-range forecasting of severe weather risk, certain methodological constraints merit consideration. The reliance on the European Severe Weather Database (ESWD) as a training dataset introduces inherent spatial reporting biases. Despite rigorous quality control, reporting density is biased in favour of more densely populated areas and is tied to the strength of national meteorological institutions. Although the ETEI mitigates this by focusing on the environmental background – effectively filling the gaps where tornadoes occur but go unreported – the initial calibration remains firmly tethered to documented events.

Another limitation is that the occurrence of convective events is unsteady through time. While appropriate for identifying large-scale teleconnections, the use of composite means thus inherently smooths the high-frequency variability and clustering tendency of severe weather events. Future research could nonetheless fruitfully explore 'probability-of-exceedance' approaches by quantifying the

shift in frequency of days exceeding the 90th percentile of ETEI rather than relying only on composite anomalies.

Although the EA-positive regime demonstrates a clear, amplified surge in the daily frequency of tornado reports during the target T + 15 to T + 30 window, Figure S3 shows that the aggregate observational signal exhibits high variance. When aggregated over the 16-day window, the "hit rate" — defined as the fraction of SSW events featuring at least one documented tornado — increases from 22% under EA-negative regimes to 35% under EA-positive regimes. While this confirms a physical enhancement of convective activity, the limited sample size of historical SSW events inherently restricts statistical significance testing on raw counts (e.g., Fisher's exact test yields $p = 0.25$). This noise underscores a fundamental reality of S2S forecasting: teleconnection-driven anomalies provide a favourable thermodynamic and kinematic baseline, but discrete convective initiation still relies on transient, synoptic-scale shortwaves that remain unpredictable at such lead times. Additionally, this observational validation is subjected to the intrinsic reporting inconsistencies within the ESWD, where daily reporting rates are modulated by population density and varying national verification protocols rather than strictly meteorological factors. Consequently, the predictive skill demonstrated here must be interpreted probabilistically rather than deterministically. The coupling between the SSW and the EA pattern reliably flags "windows of opportunity" featuring a substantially elevated baseline risk, but it does not guarantee the outbreak of specific events on specific days, thereby warranting a cautious, ensemble-based approach to operational S2S implementation.

Lastly, although the projection onto satellite-era EOFs ensures structural consistency, the underlying ERA5 geopotential field during the pre-satellite era (1950–1978) remains more poorly constrained by direct observations. Our stratospheric detection algorithm is designed to be conservative, but users should acknowledge that the NAM index in the pre-1979 period carries a higher degree of reanalysis-driven uncertainty than after 1979.

## 4.4. Operational implications for S2S forecasting

The results highlighted in this study represent a potentially significant enhancement to the current sub-seasonal and seasonal weather forecasting capacity in Europe. Current operational severe weather assessments, which are conducted in Europe by organisations such as ESTOFEX or national meteorological services, are largely confined to synoptic-scale windows, typically not exceeding 7 days. Our analysis demonstrates that a window of predictability for severe convective environments exists beyond this time envelope.

By monitoring the stratospheric polar vortex at 10 hPa, forecasters can identify the onset of a potential downward-propagating NAM anomaly. However, our findings underscore that this stratospheric signal must be interpreted through the lens of the tropospheric background state. Specifically, the East Atlantic (EA) pattern serves as a critical diagnostic tool: monitoring the EA phase at the onset of a major SSW allows for the identification of high-risk probability windows for tornado-generating storms 3 to 4 weeks in advance.

This multi-tiered forecasting approach, i.e., the combination of stratospheric monitoring for long-lead kinematic potential with EA-regime tracking for thermodynamic feasibility, enables the issuance of probabilistic S2S outlooks for severe convection. Such lead times can provide essential support for resource allocation to first-responder authorities and infrastructure management, effectively bridging the gap between medium-range synoptic forecasts and seasonal climate outlooks.

## Conclusions

This study introduced the European Tornado Environment Index (ETEI), a continuous daily proxy for severe convective potential calibrated using a Poisson GLM and reconstructed for the 1950–2025 period. We demonstrate that stratosphere–troposphere coupling following major Sudden Stratospheric Warming events (SSWs) does not act as a uniform driver of European severe weather. Instead, the surface response is governed by non-linear interactions with pre-existing tropospheric regimes. On that basis, our analysis offers three primary contributions to climate dynamics:

1. Regional sensitivity: we establish that the European convective environment is primarily sensitive to low-level kinematic organisation rather than deep-layer shear. This necessitates an additive regional approach to the formulation of severe weather proxies, fundamentally distinct from the multiplicative approach to TEIs in North America.
2. Limitations of bulk analysis: we show that the downward propagation of the stratospheric NAM signal generates a profound but highly variable sub-seasonal response. Aggregate composite methodologies effectively mask this variability, highlighting the need for more finely stratified approaches when assessing extreme weather.
3. The East Atlantic pattern as a gatekeeper: we identify the EA pattern as the crucial regulator of this stratosphere–troposphere coupling. An EA-negative regime leads to widespread suppression of tornadic potential through continental blocking, whereas an EA-positive background couples synergistically with the SSW-induced jet displacement. This combination provides the thermodynamic instability and kinematic shear necessary for amplifying the risk of severe convection, particularly over the Iberian Peninsula, France, and the Mediterranean Basin.

By integrating stratospheric monitoring with tropospheric teleconnection patterns, this research establishes a physically grounded framework for anticipating high-impact severe weather three to four weeks in advance. This conditional approach bridges the gap between stratospheric dynamics and ground-level extremes, providing a foundation for more reliable sub-seasonal to seasonal (S2S) operational forecasting of severe convection and tornado hazards in Europe.

## Declarations

# Conflict of interests

The authors have no relevant financial or non-financial interests to disclose.

# Funding

The authors declare that no funds, grants, or other support were received during the preparation of this manuscript.

# Author Contributions

All authors contributed to the study conception and design. Material preparation, data collection and analysis were performed by Matthieu Lacroix. The first draft of the manuscript was written by Matthieu Lacroix and all authors commented on previous versions of the manuscript. All authors read and approved the final manuscript.

# Data Availability statement

The datasets generated during and/or analysed during the current study are available from the corresponding author on reasonable request.

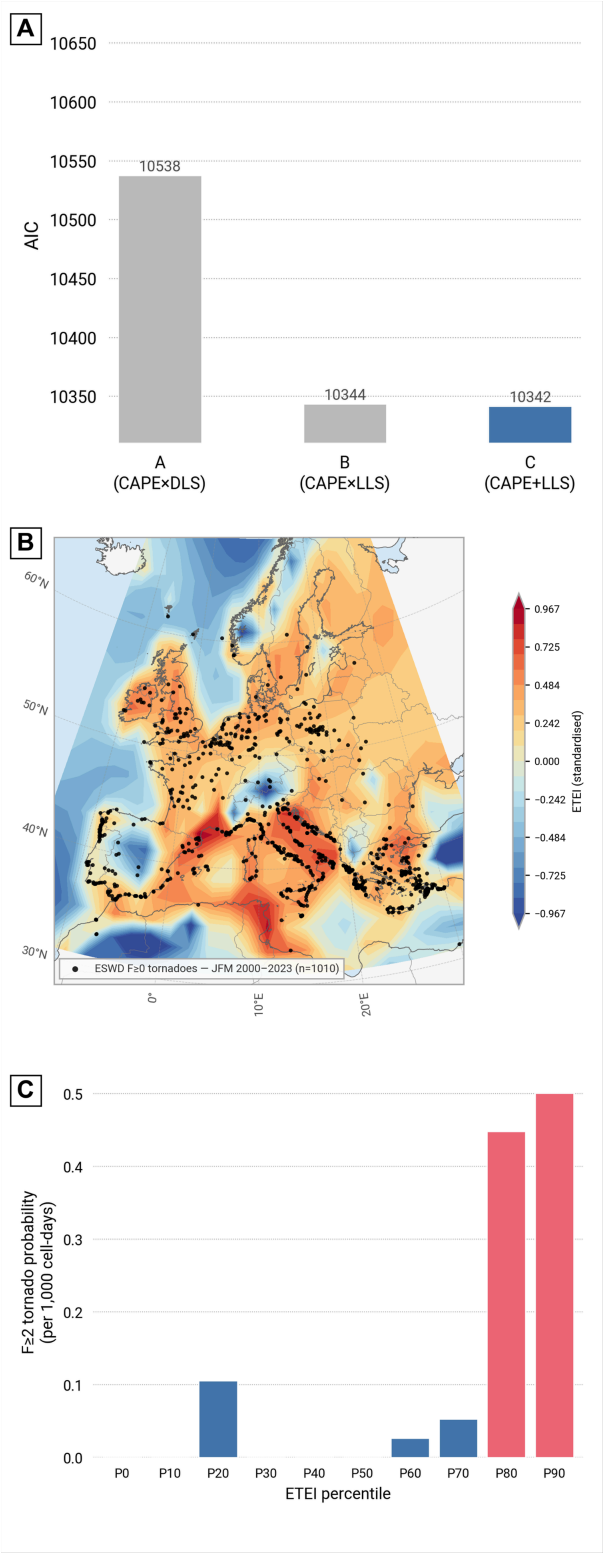
## References

1. Antonescu B, Schultz DM, Holzer A, Groenemeijer P (2017) Tornadoes in Europe: An Underestimated Threat. Bull Am Met Soc 98(4):713–728. https://doi.org/10.1175/BAMS-D-16-0171.1
2. Baldwin MP, Dunkerton TJ (2001) Stratospheric harbingers of anomalous weather regimes. Science 294(5542):581–584. https://doi.org/10.1126/science.1063315
3. Baldwin MP, Thompson DWJ (2009) A critical comparison of stratosphere–troposphere coupling indices. Quart J Roy Met Soc 135(644):1661–1672. https://doi.org/10.1002/qj.479
4. Bell B, Hersbach H, Simmons A, Berrisford P, Dahlgren P, Horányi A, Muñoz-Sabater J, Nicolas J, Radu R, Schepers D, Soci C, Villaume S, Bidlot J, Haimberger L, Woollen J, Buontempo C, Thépaut J (2021) The ERA5 global reanalysis: Preliminary extension to 1950. Quart J Roy Met Soc 147(741):4186–4227. https://doi.org/10.1002/qj.4174
5. Brooks HE, Lee JW, Craven JP (2003) The spatial distribution of severe thunderstorm and tornado environments from global reanalysis data. Atmos Res 67–68:73–94. https://doi.org/10.1016/S0169-8095(03)00045-0
6. Burnham KP, Anderson DR (2004) Model Selection and Multimodel Inference. Springer New York. https://doi.org/10.1007/b97636
7. Butler AH, Sjoberg JP, Seidel DJ, Rosenlof KH (2017) A sudden stratospheric warming compendium. Earth Syst Sci Data 9(1):63–76. https://doi.org/10.5194/essd-9-63-2017

8. Charlton AJ, Polvani LM (2007) A new look at stratospheric sudden warmings. Part I: climatology and modeling benchmarks. J Clim 20(3):449–469. https://doi.org/10.1175/JCLI3996.1
9. Comas-Bru L, McDermott F (2014) Impacts of the EA and SCA patterns on the European twentieth century NAO–winter climate relationship. Quart J Roy Met Soc 140(679):354–363. https://doi.org/10.1002/qj.2158
10. Domeisen DIV, Butler AH (2020) Stratospheric drivers of extreme events at the Earth's surface. Comm Earth Environ 1(1):59. https://doi.org/10.1038/s43247-020-00060-z
11. Domeisen DIV, Butler AH, Charlton-Perez AJ, Ayarzagüena B, Baldwin MP, Dunn-Sigouin E, Furtado JC, Garfinkel CI, Hitchcock P, Karpechko A, Yu KH, Knight J, Lang AL, Lim E, Marshall A, Roff G, Schwartz C, Simpson IR, Son S, Taguchi M (2019) The role of the stratosphere in subseasonal to seasonal prediction: 1. Predictability of the stratosphere. J Geophys Res: Atmos 125(2). https://doi.org/10.1029/2019JD030920. e2019JD030920
12. Doswell CA, Brooks HE, Maddox RA (1996) Flash flood forecasting: an ingredients-based methodology. Weath Forecasting 11(4):560–581. https://doi.org/10.1175/1520-0434(1996)011%253C0560:FFFAIB%253E2.0.CO;2
13. Groenemeijer P, Kühne T (2014) A climatology of tornadoes in Europe: results from the European Severe Weather Database. Month Weath Rev 142(12):4775–4790. https://doi.org/10.1175/MWR-D-14-00107.1
14. Hersbach H, Bell B, Berrisford P, Hirahara S, Horányi A, Muñoz-Sabater J et al (2020) The ERA5 global reanalysis. Quart J Roy Met Soc 146(730):1999–2049. https://doi.org/10.1002/qj.3803
15. Kidston J, Scaife AA, Hardiman SC, Mitchell DM, Butchart N, Baldwin MP, Gray LJ (2015) Stratospheric influence on tropospheric jet streams, storm tracks and surface weather. Nat Geosci 8(6):433–440. https://doi.org/10.1038/ngeo2424
16. Lacroix M, Couto FT, Gunnell Y (2026a) Intense autumn and winter tornadoes in a region of low convective available potential energy: Insights from western continental Europe (1940–2022). Atmos Res 109169. https://doi.org/10.1016/j.atmosres.2026.109169
17. Lacroix M, Couto FT, Gunnell Y (2026b) Dual drivers of European severe weather: How the NAO and low-frequency climate variability modulate the seasonal transition from shear- to CAPE-dominated tornadogenesis. Weath Clim Extr 53:100920. https://doi.org/10.1016/j.wace.2026.100920
18. North GR, Bell TL, Cahalan RF, Moeng FJ (1982) Sampling errors in the estimation of empirical orthogonal functions. Month Weath Rev 110(7):699–706. https://doi.org/10.1175/1520-0493(1982)110%253C0699:SEITEO%253E2.0.CO;2
19. Piper DA, Kunz M, Allen JT, Mohr S (2019) Investigation of the temporal variability of thunderstorms in central and western Europe and the relation to large-scale flow and teleconnection patterns. Quart J Roy Met Soc 145(725):3644–3666. https://doi.org/10.1002/qj.3647
20. Púčik T, Groenemeijer P, Rýva D, Kolář M (2015) Proximity soundings of severe and nonsevere thunderstorms in central Europe. Month Weath Rev 143(12):4805–4821. https://doi.org/10.1175/MWR-D-15-0104.1

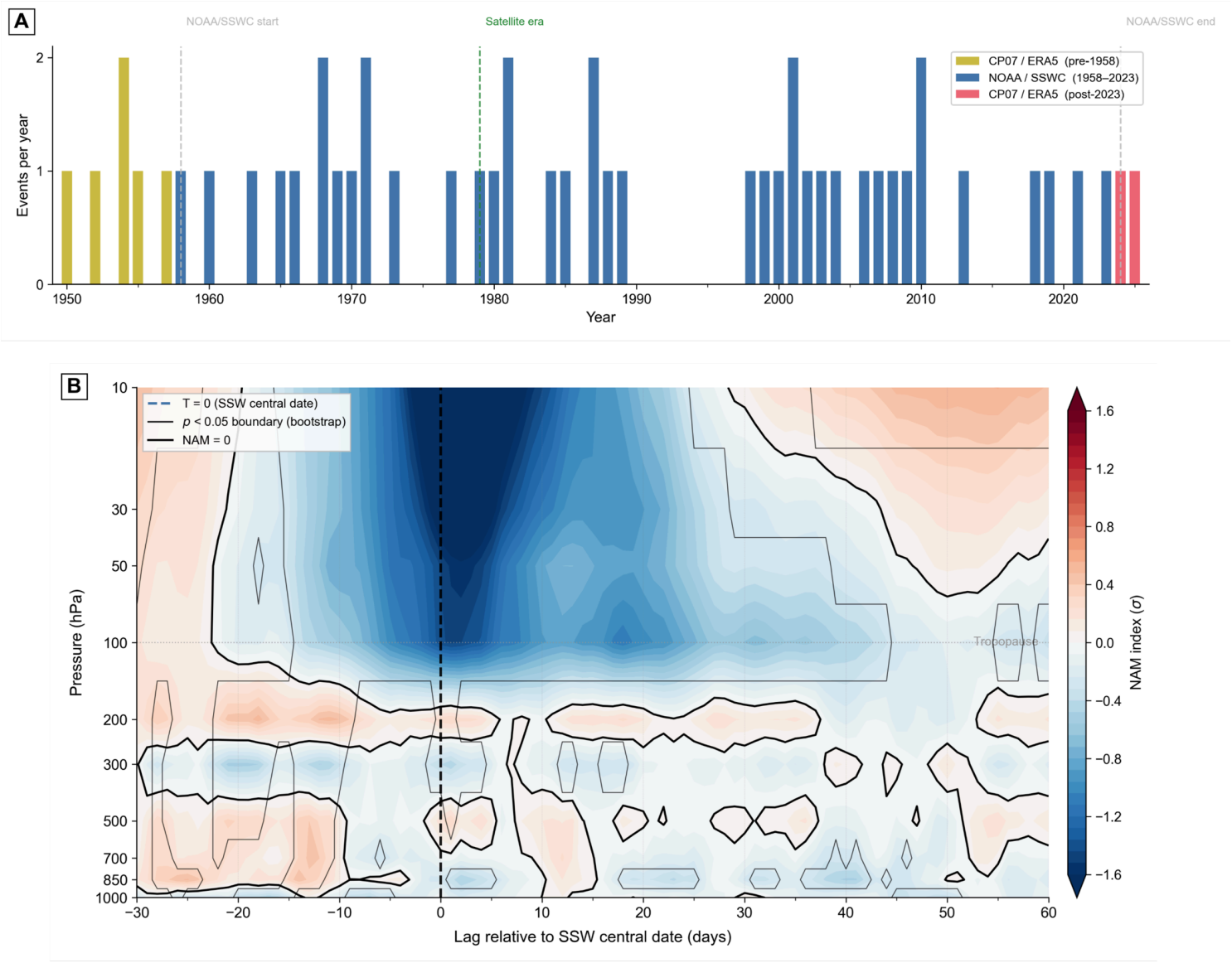
21. Schultz DM, Schumacher PN, Doswell CA (2000) The intricacies of instabilities. Month Weath Rev 128(12):4143–4148. https://doi.org/10.1175/1520-0493(2000)129%253C4143:TIOI%253E2.0.CO;2
22. Taszarek M, Allen JT, Groenemeijer P, Edwards R, Brooks HE, Chmielewski V, Enno E (2020) Severe convective storms across Europe and the United States. Part I: Climatology of lightning, large hail, severe wind, and tornadoes. J Clim 33(23):10239–10261. https://doi.org/10.1175/JCLI-D-20-0345.1
23. Taszarek M, Pilguj N, Allen JT, Gensini V, Brooks HE, Szuster P (2020) Comparison of convective parameters derived from ERA5 and MERRA2 with rawinsonde data over Europe and North America. J Clim 1–55. https://doi.org/10.1175/JCLI-D-20-0484.1
24. Thompson DWJ, Wallace JM (2000) Annular modes in the extratropical circulation. Part I: Month-to-month variability. J Clim 13(5):1000–1016. https://doi.org/10.1175/1520-0442(2000)013%253C1000:AMITEC%253E2.0.CO;2
25. Tippett MK, Lepore C, L'Heureux ML (2022) Predictability of a tornado environment index from El Niño–Southern Oscillation (ENSO) and the Arctic Oscillation. Weath Clim Dyn 3(3):1063–1075. https://doi.org/10.5194/wcd-3-1063-2022
26. Tippett MK, Sobel AH, Camargo SJ (2012) Association of U.S. tornado occurrence with monthly environmental parameters. Geophys Res Lett 39(2):2011GL050368. https://doi.org/10.1029/2011GL050368
27. Tippett MK, Sobel AH, Camargo SJ, Allen JT (2014) An empirical relation between U.S. tornado activity and monthly environmental parameters. J Clim 27(8):2983–2999. https://doi.org/10.1175/JCLI-D-13-00345.1
28. Tripathi OP, Charlton-Perez A, Sigmond M, Vitart F (2015) Enhanced long-range forecast skill in boreal winter following stratospheric strong vortex conditions. Environ Res Lett 10(10):104007. https://doi.org/10.1088/1748-9326/10/10/104007
29. Yu Y, Cai M, Garfinkel C (2022) Editorial: Stratosphere–troposphere coupling and its role in surface weather predictability. Front Earth Sci 10:885934. https://doi.org/10.3389/feart.2022.885934

# Figures



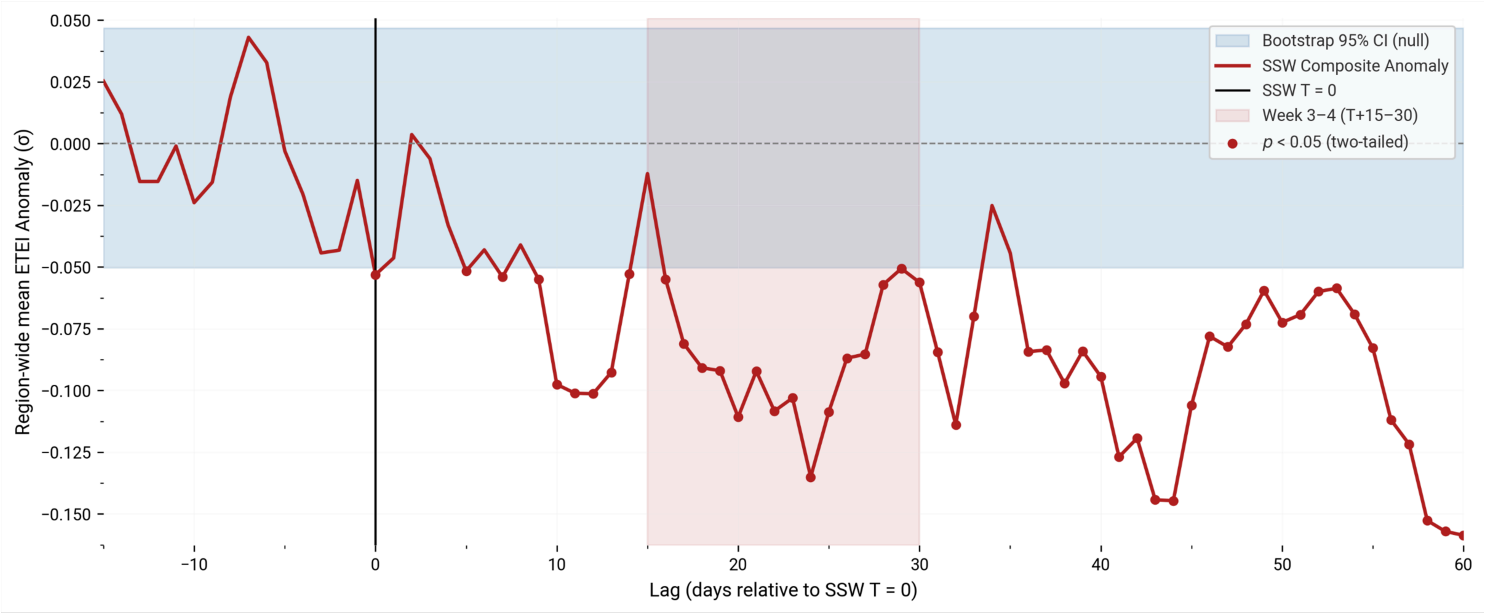

## Figure 1

Legend not included with this version



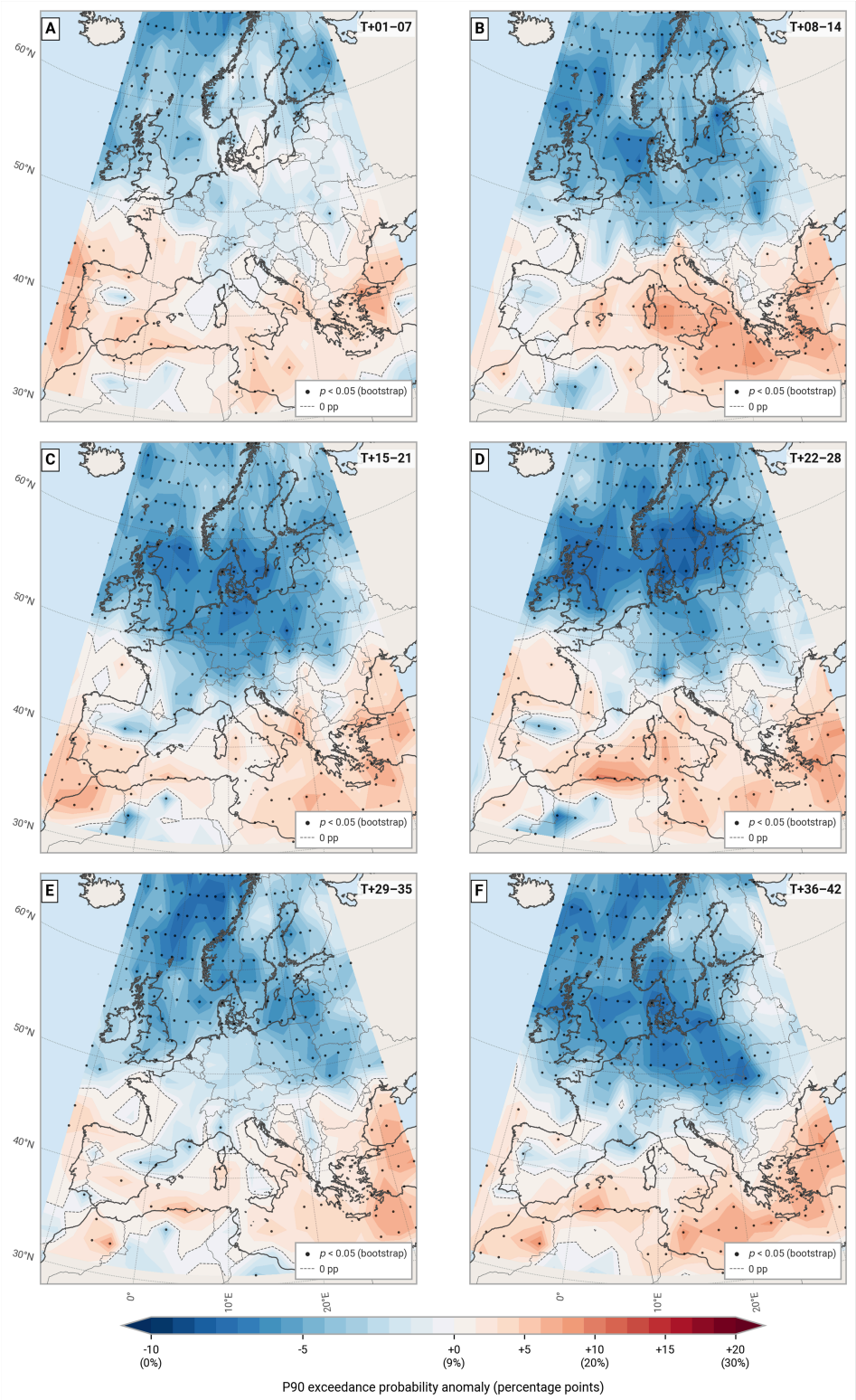

## Figure 2

Legend not included with this version



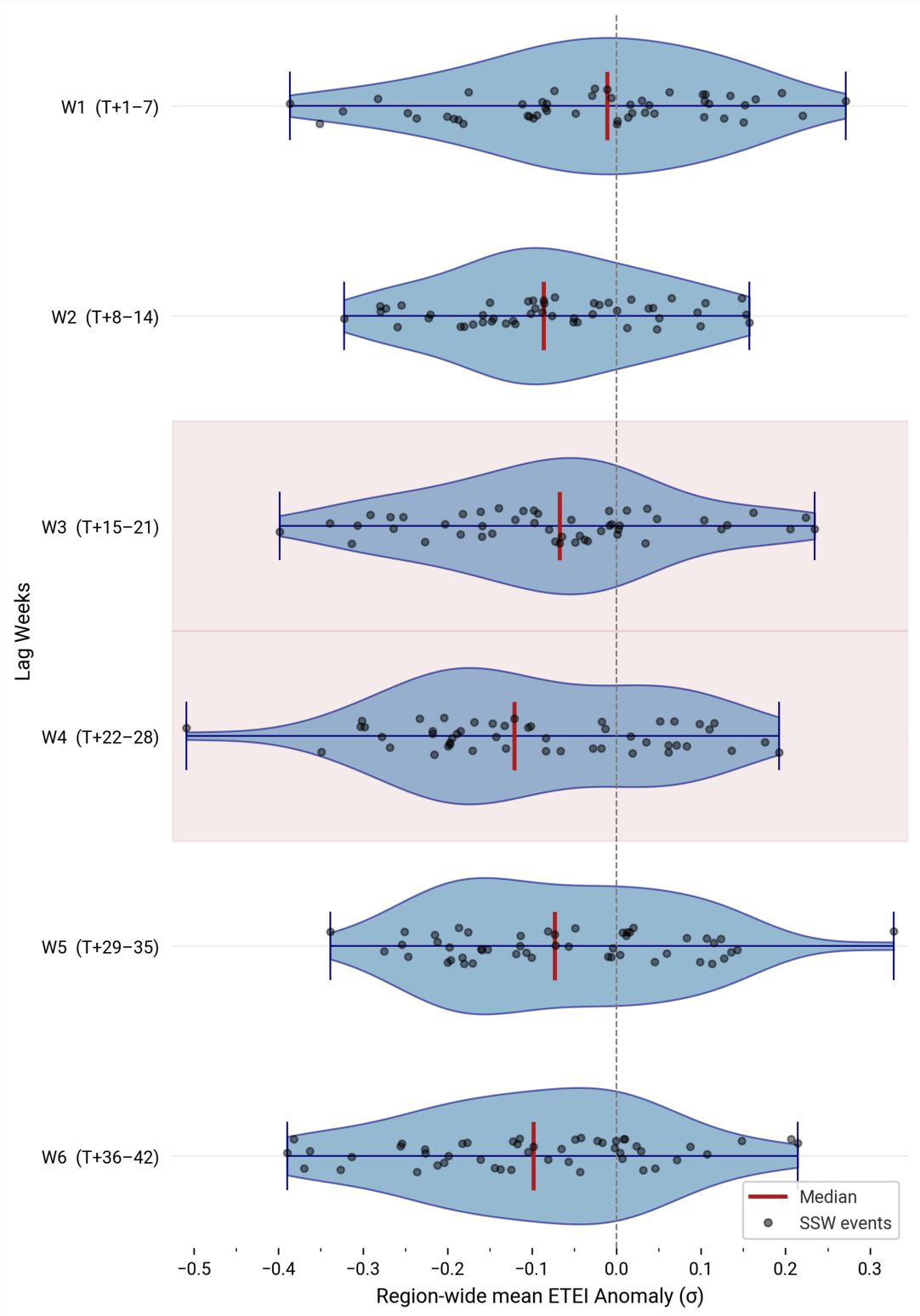

## Figure 3

Legend not included with this version




## Figure 4

Legend not included with this version




## Figure 5

Legend not included with this version

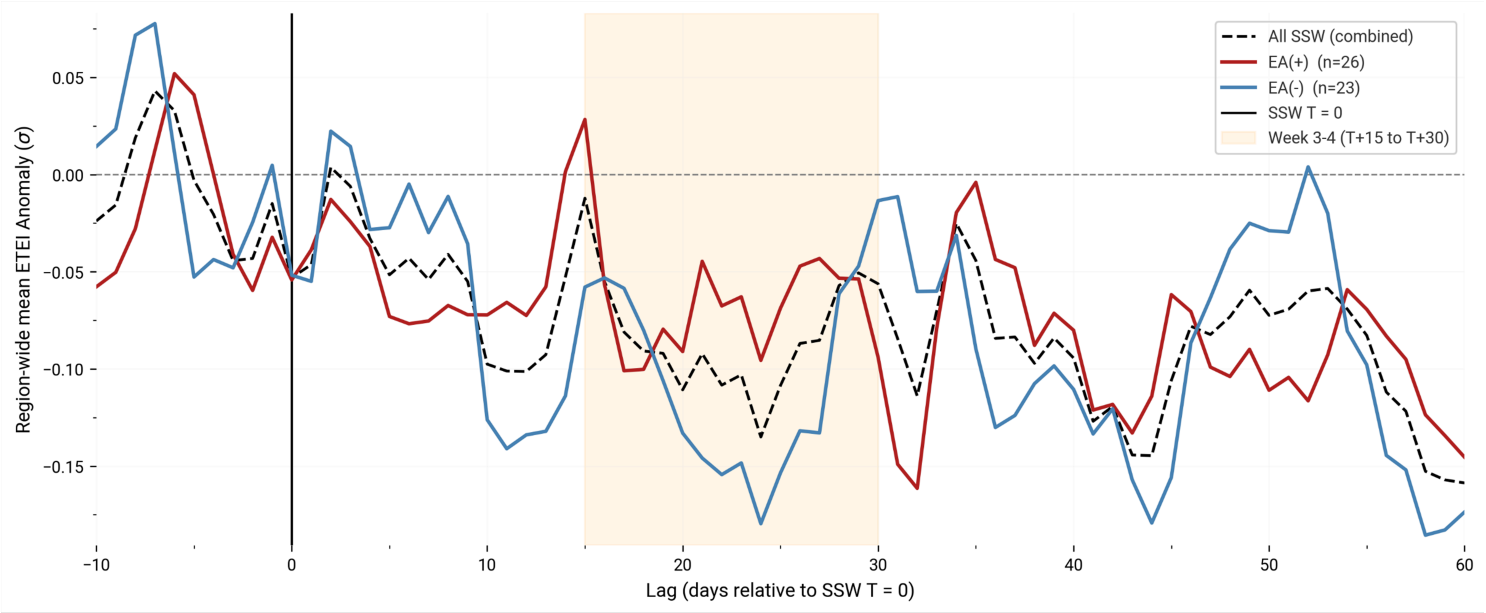



**Figure 6**

Legend not included with this version

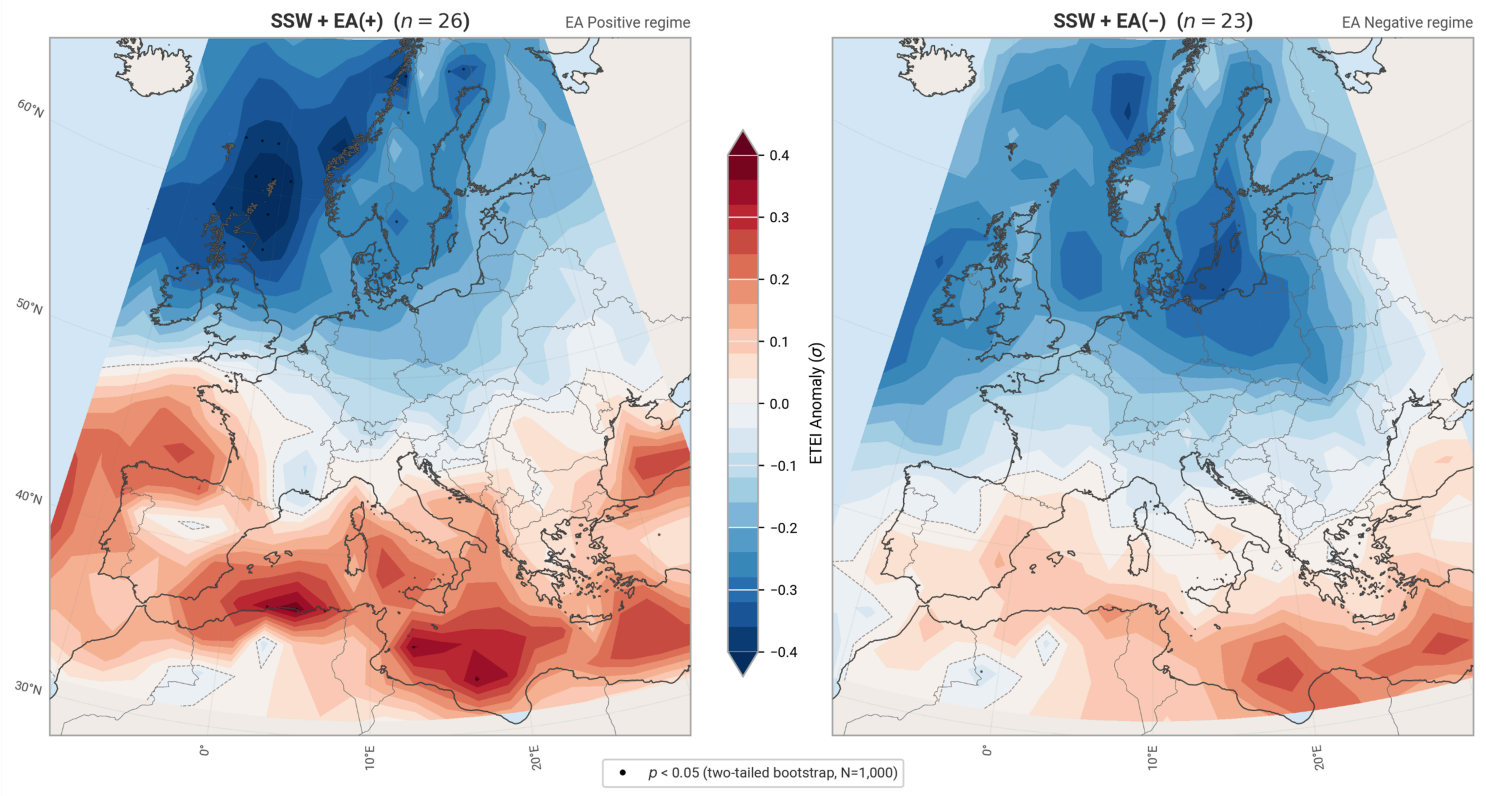



**Figure 7**

Legend not included with this version

# Supplementary Files

This is a list of supplementary files associated with this preprint. Click to download.

- TABLE1.docx
- FinalSupplementmaterial.docx